Journal of Applied Polymer Science

Graphene/Poly(styrene-*b*-isoprene-*b*-styrene) Nanocomposite Optical Actuators

Seema Ansari*, Muralidharan Malamal Neelanchery, Deepthi Ushus
Centre for Materials for Electronics Technology, Thrissur, Kerala 680581, India
Correspondence to: S. Ansari (E-mail: seema@cmet.gov.in or seemacmet@gmail.com)

ABSTRACT: This article presents an optomechanical actuator, which is driven by infra red (IR) radiation. The actuator is a nanocomposite-containing graphene platelets embedded in poly(styrene-*b*-isoprene-*b*-styrene) (SIS) matrix. 0.1 mm thick free-standing nanocomposite films are fabricated by a simple process of solvent casting. We demonstrate that graphene/SIS nanocomposite contracts on irradiation with IR radiation under strained conditions, whereas expansion behavior was exhibited by them when no prestrain is applied. A maximum photomechanical stress of 28.34 kPa and strain upto 3.1% was obtained for these nanocomposite actuators. We have also studied the mechanical characteristics and thermal degradation of these nanocomposite actuators. © 2013 Wiley Periodicals, Inc. J. Appl. Polym. Sci. 130: 3902–3908, 2013

KEYWORDS: composites; optical properties; sensors and actuators; nanotubes; graphene and fullerenes

Received 17 April 2013; accepted 14 June 2013; Published online 2 July 2013
DOI: 10.1002/app.39666

INTRODUCTION

Actuation is the ability of various materials to change their mechanical properties and dimensions when an appropriate external stimulus is applied. By absorbing the energy from an external stimulus, these materials undergo internal state of changes thus leading to mechanical change much larger than the initial input. The various types of actuators include electromechanical, electromagnetic, electrodynamic, photomechanical, fluid mechanical, pneumatic, hydraulic, and so on.[1–2] Most of the usually used actuators are driven by an external electric power source like a battery or even a voltage generator. These actuators need high voltages for actuation and use much energy. When actuation system is to be operated in or near the human body or other biological systems, the use of electrical power devices can induce problems. Even with greater advancement in the battery technologies, batteries still belong to the most spacious and heavy parts in an electrical assembly. Moreover, the toxicity of these battery materials cannot be fully avoided and much attention has to be given to sealing of the battery. Additionally, these devices need either battery recharge or frequent replacement, which can be very troublesome. Hence, optical-induced actuators have great preference in biomedical field to any other kind.[3] Photo-induced actuation technologies offer many advantages over traditional electrically driven actuators, such as remote energy transfer, remote controllability, better scalability, low electromagnetic noise, easy construction, and capability of working in harsh environment.

The best known materials used today for actuation are piezoelectric, electrostrictive, ferroelectric materials, shape memory alloys, materials, and conducting polymers. Of these materials, some have one-way response, while others give reversible response to a given stimulus. For example, most of the shape memory system works only in one direction and requires a reset after the actuation. Only very few systems can reversibly actuate and then return back to the equilibrium shape once the stimulus is removed. Photomechanical materials that have responses near near-infrared (NIR) wavelength region have various potential applications such as telecommunication, thermal imaging, remote sensing, thermal photovoltaics, and solar cells.

Many researchers have reported liquid crystalline polymer materials for photomechanical actuators. Polymers with photo-responsive group incorporated were also studied for photomechanical actuators. A polymer benign to light stimulus can also be made to photoactuators by blending with one or more photo-absorbing materials to impart a new physical response leading to the photo actuation process.[4–12]

Polymer nanocomposites attract considerable interest because of the excellent electrical, thermal, optical, and mechanical properties encountered with only a small quantity of nanofiller incorporated to the polymer matrix. Polymer nanocomposites find wide applications in various industries ranging from construction to aerospace. Photomechanical actuation is one of the unique applications of this class of materials.

Graphene is a promising "new" material that could revolutionize the world of electronics, technology, manufacturing, and more. Graphene's impressive properties and characteristics are responsible for most of its practical applications.[13,14] Graphene-based fillers have been used in polymer nanocomposites and hold potential for a variety of possible applications.[15–22] Graphene-based composites find applications in a large number of fields, including actuators, sorbent/filter/medical applications, lightweight high-strength structural components, and electrically or thermally conducting nanocomposites.[23–28]

Poly(styrene-*b*-isoprene-*b*-styrene) (SIS) is a triblock copolymer belonging to the family of thermoplastic elastomers (TPEs). This polymer has many of the properties of vulcanized rubbers but can be molded and extruded on conventional thermoplastic processing equipments. SIS when blended with carbon nanotube (CNT) is found to have photomechanical actuation.[11] However, the photomechanical properties of SIS nanocomposites are not much understood when compared to other photomechanical polymer nanocomposites like CNT/polydimethylsiloxane (PDMS), and so on.[1,7,10–12] Recently, graphene is found to be an excellent filler material for polymer composite-based light-triggered actuators.[29–32] In this work, SIS/graphene nanocomposites were developed and its photomechanical properties were studied.

EXPERIMENTAL

Preparation of Graphene

Preparation of graphene sheets includes two steps, namely, the oxidation of natural graphite flakes (94.1% C + 50 Mesh, Hind Minerals, Mumbai, India) using an improved Hummers method of synthesis[33] and rapid thermal expansion process. To prepare graphite oxide, a 9:1 mixture of H_2SO_4 (98% GR, Merck India, Mumbai, India)/H_3PO_4 (85% pure, Merck India, Mumbai, India) (678:75 ml) was added to a mixture of 1 mol of graphite flakes and 0.433 mol $KMnO_4$ (99%, Merck India, Mumbai, India), kept in an ice bath slowly with stirring. After 24 h of stirring about 450 mL of ice water was added to the reaction mixture. During addition of ice water, the temperature of the system rises to about 98°C. After complete addition of water it was again stirred for 2 h. Then to the mixture 20 mL of H_2O_2 (30%) was added. The stirring process continued for another 2 h so that the temperature of the system reaches around room temperature. The reaction mixture was centrifuged (4000 rpm, 20 min.) and washed five times with 5% HCl solution followed by washing with distilled water. The resultant graphite oxide was then exfoliated in water by ultrasonication using bath sonicator to form graphene oxide (GO).

Thermal reduction of GO was achieved by placing dried GO into a crucible and inserting the same into a muffle furnace preheated to 1000°C. The sample was held in the furnace for about 30 s to 1 min.

Preparation of Graphene/SIS Nanocomposite

Graphene–SIS nanocomposites having various filler concentration (0–2.5 wt %) were prepared by solvent casting method. 20 wt % SIS solution was prepared by dissolving 2 g of SIS in 10 mL of Toluene (Merck India, Mumbai, India) by sonication using bath sonicator (Frequency 40KHz, Powersonic 405, Hwashin Technology Co., Seoul, Republic of Korea), for about 2 h. Depending upon the graphene loading in SIS, required quantity of graphene was dispersed in toluene by sonication using a bath sonicator for 4–5 h until a uniform dispersion of graphene is obtained. To the graphene dispersion under sonication, SIS solution in toluene was added and mixed together by further sonication for 1 h. During the mixing, a coating of SIS on graphene particles will take place thus preventing the settling of the graphene particles. The resultant mixture was casted on a rectangular mould and samples were air dried at 50°C to obtain 0.1 mm thick graphene–SIS nanocomposite sheets.

Characterization

Graphene powder obtained after 5 h of sonication in toluene was characterized by X-ray diffraction (XRD) studies (D5005, Bruker, Germany, using Cu-Kα radiation), Raman spectroscopy with a 514 nm laser excitation (LabRAM, Horiba Jobin Yvon, Japan), Fourier transform infra red spectroscopy (FTIR, Avatar 370, Thermo Nicolet, Germany), scanning electron microscopy (SEM, SU 6600, Hitachi, Japan), and transmission electron microscopy (HR TEM, JEM 2100, JEOL, Japan).

SEM of fractured surface of graphene/SIS nanocomposite was carried out using variable pressure field emission SEM. Optical microscopy (BX 51, Olympus, Japan) of 1.5 wt % graphene/SIS nanocomposites was done. FTIR spectroscopy and Thermogravimetric analysis (TGA, SDT Q500, TA Instruments, New Castle, DE) under nitrogen at a heating rate of 10°C/min of graphene/SIS nanocomposites were carried out. Mechanical properties of the composites as per ISO 37 (type 4) standard (Universal Testing Machine, Shimadzu, Japan) were also measured.

Photomechanical Actuation of Graphene/SIS Composite

Strips of 15 mm × 5 mm sizes were cut from the graphene/SIS nanocomposite sheets. The thickness of the sample was 0.1 mm. Actuation was measured by using 1205A 5.0 N *in vitro* Muscle test system (Aurora Scientific Inc., Canada) which consists of dual mode system with lever arm (model 305 C) and 805A *in vitro* test apparatus. The tips of the strips were placed between the grips of *in vitro* Muscle test system. The length between the grips of the test apparatus was fixed at 10 mm. The infrared lamp, Philips, Germany, with red filter was used as the light source, which is positioned at 25 cm away from the sample and an exposure time of 15 s is fixed. The intensity of the IR light is measured using power meter (Newport 1916C, USA) with detector (Newport 818-SL, USA). The intensity was calculated and it was found to be 22 mW/cm^2. Both the strain and the stress were measured at various prestrains.

RESULTS AND DISCUSSIONS

Characterization of Graphene and Graphene/SIS Nanocomposites

GO shows an XRD peak at $2\theta = 11.2°$ [Figure 1(a)] corresponding to a *d*-spacing of 0.79 nm. The intercalation of the various functional group and solvent molecules led to the increased *d* spacing in GO when compared to graphite. Graphene shows no characteristic peak of either GO or graphite.

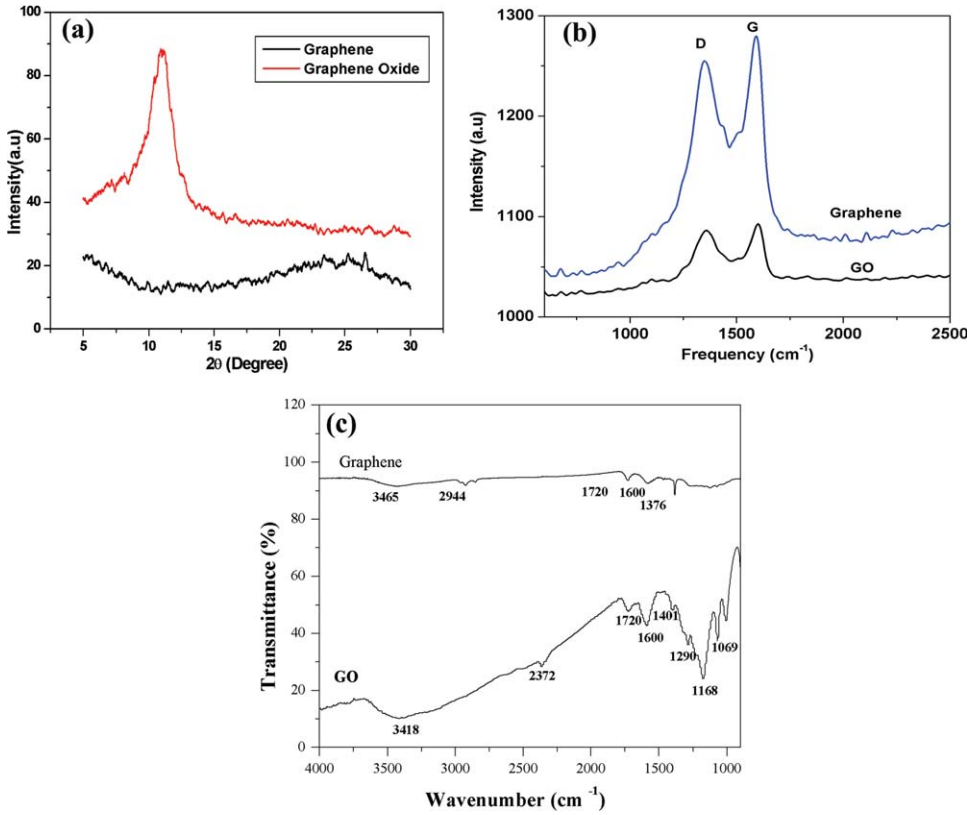

Figure 1. (a) XRD pattern, (b) Raman spectra, and (c) FTIR spectra of graphene and GO. [Color figure can be viewed in the online issue, which is available at wileyonlinelibrary.com.]

This indicates high degree of exfoliation of graphitic layers and almost complete reduction of GO into graphene.

In the Raman spectra, both GO and graphene show prominent D and G bands [Figure 1(b)]. G band is because of the first order scattering of E_{2g} mode observed for sp^2-hybridized carbon atoms and the D band is because of the breathing mode vibration of aromatic rings and requires defects for its activation. Raman spectrum of GO shows D band at 1357 cm^{-1} and G band at a frequency of 1605 cm^{-1} and that of graphene is at 1350 and 1592 cm^{-1}, respectively. The blue shift of the graphitic G band (1580 cm^{-1} for graphite) in GO is reversed back in graphene along with the sharpening of the G band, which indicates the regaining of sp^2 hybridized state. G band in graphene is highly prominent because it retains their graphitic network after thermal reduction. In GO, lot of hydroxyl and epoxy groups are present which in turn decreases the amount of aromatic rings, thereby diminishing the intensity of D band. The reduced sp^2 hybridized nature and the presence of more sp^3-hybridized carbon in GO causes the reduction of intensity and broadening of G band. Once GO is reduced, most of those oxygenated groups are eliminated, reintroducing aromaticity and electrical conductivity in the structure. The strong D band intensity of graphene compared to that of GO showed that the reduction process improves the aromaticity to a greater extend.

FTIR spectrum of GO shows a broad peak at 3418 cm^{-1} related to water –O–H stretching vibration [Figure 1(c)]. Other significant peaks in GO are 1069 (–C–O stretching), 1168 (epoxy group), 1290 (carboxyl O=C–O), 1401 (–O–H bending), 1600 (skeletal vibrations from unoxidized graphitic domains), and 1720 cm^{-1} (stretching vibrations from C=O). All these peaks indicate that oxidation of graphite introduces epoxide and hydroxide groups on the graphitic network. Upon thermal reduction of GO to graphene no significant peak is observed which gives strong evidence for the hydrophobic nature of graphene.[34–37]

The SEM of the graphene powder obtained after 5 h of sonication in toluene is given in Figure 2(a). It can be observed that graphitic layers are exfoliated to get thin graphene sheets. It can also be seen that by large the graphene sheet dimension is in the range of 2–3 μm. These large size graphene sheets can harvest maximum infrared light and can be uniformly transferred to the polymer matrix. The TEM image of the graphene prepared by chemical route is given in Figure 2(b) which shows single to few layer graphene.

The optical micrograph [Figure 3(a)] of graphene/SIS nanocomposite reveals that graphene is distributed throughout the entire matrix, however, some agglomerated graphene sheets were also observed. During the preparation of nanocomposites, SIS solution was added to the graphene dispersion under sonication, which leads to the formation of coating of SIS on graphene platelets. This prevents the settling and agglomeration of graphene platelets; thus, achieving uniform dispersion of graphene in SIS matrix. In order to confirm this, we have studied the settling rate of graphene in SIS solution in toluene. It is observed that the solution is stable for more than 4 days. The

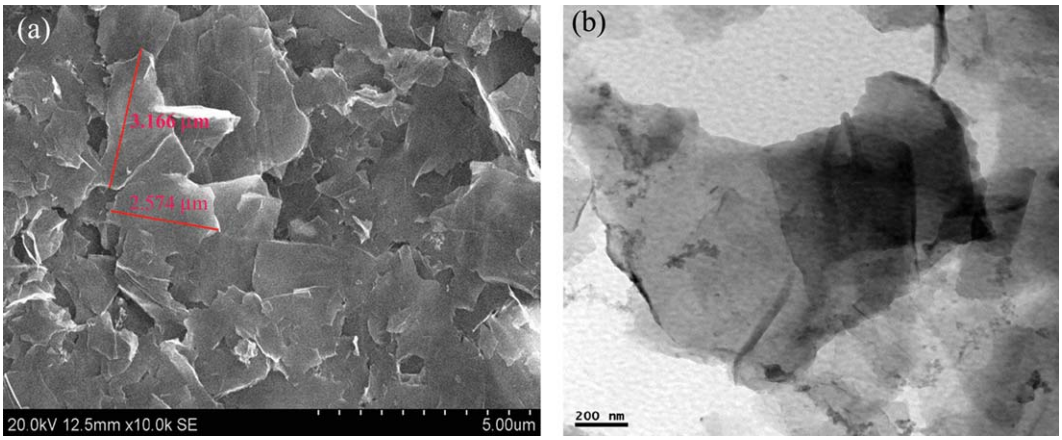

Figure 2. (a) SEM of graphene sonicated in toluene for 5 h and (b) TEM of the graphene prepared. [Color figure can be viewed in the online issue, which is available at wileyonlinelibrary.com.]

graphene/SIS nanocomposite was fractured in liquid nitrogen and the SEM of the fractured surface is shown in Figure 3(b). The graphene sheets protruding from the matrix are visible in the SEM.

Graphene shows a slow thermal degradation pattern and there is no significant weight loss at a temperature range of 50°C–200°C, which means that most of the oxygen-containing groups on GO is removed during thermal reduction. The total mass loss for graphene is 24.85 wt % from 50°C to 600°C. TGA of graphene nanocomposite shows that graphene has improved the thermal stability of the SIS matrix [Figure 3(c)]. FTIR spectra of SIS and SIS/graphene nanocomposite are shown in Figure 3(d). The peaks at 2921 cm^{-1} represent the asymmetric stretch of CH_2 alkyl chains and peak at 1444 cm^{-1} shows CH_2–CH_3 bending. 1373 cm^{-1} absorbance peak shows CH_3 bending while peak at 838 cm^{-1} indicates C–H bending of phenyl ring substitution. Peaks at 752 and 700 cm^{-1} show the C–H bending in alkene and alkyne, respectively.

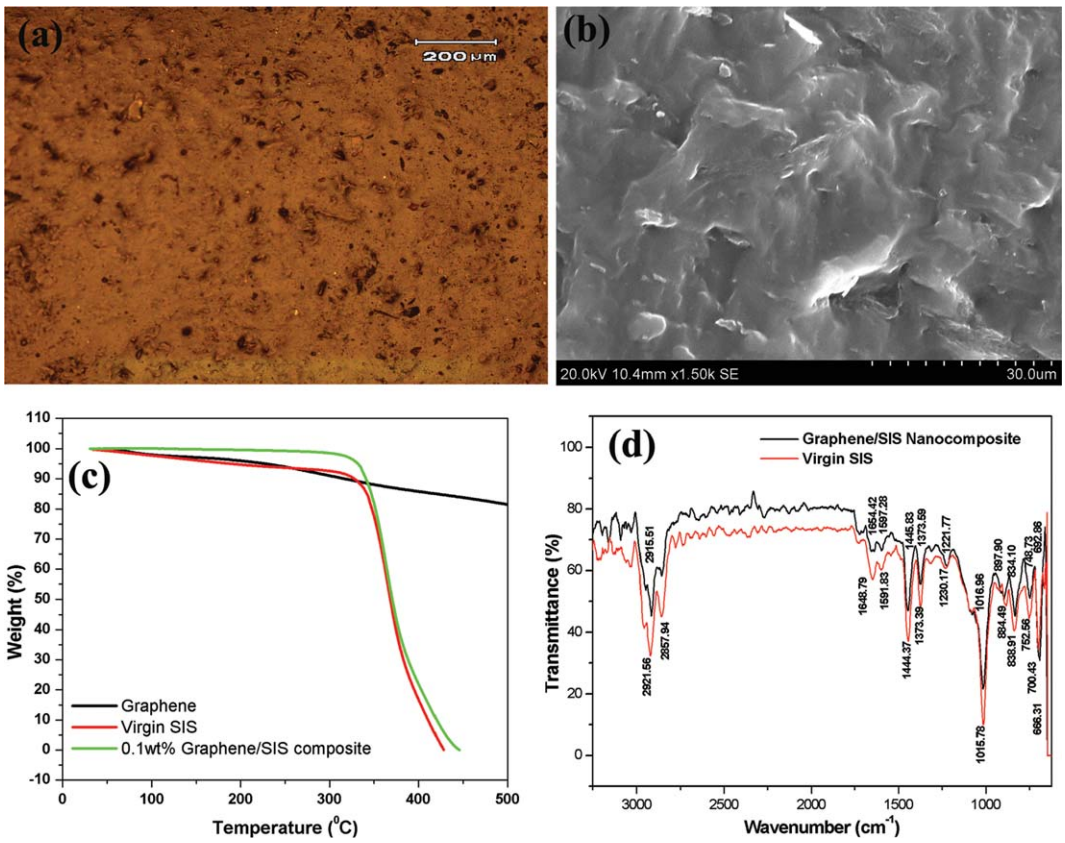

Figure 3. (a) Optical micrograph, (b) scanning electron micrograph, (c) thermogram, and (d) FTIR spectra of SIS and graphene/SIS nanocomposite. [Color figure can be viewed in the online issue, which is available at wileyonlinelibrary.com.]

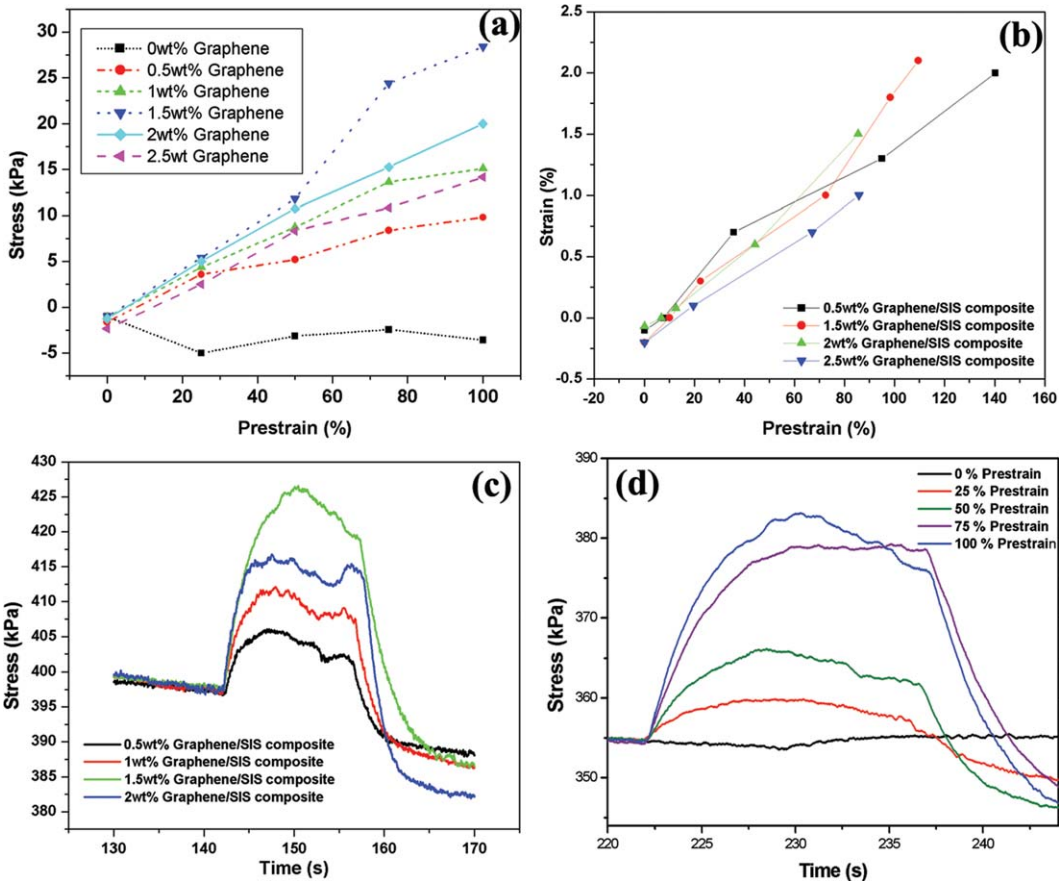

Figure 4. (a) Photomechanical stress and (b) photomechanical strain of graphene/SIS nanocomposites at various prestrain; (c) stress change of graphene/SIS nanocomposite at different graphene loading at 100% prestrain; and (d) stress changes of 1.5 wt % graphene/SIS nanocomposites at various prestrain. [Color figure can be viewed in the online issue, which is available at wileyonlinelibrary.com.]

Photomechanical Characteristics of Graphene/SIS Nanocomposites

Without any prestrain, virgin SIS, and graphene/SIS nanocomposites show expansion with infra red (IR) illumination (Figure 4). The power of IR radiation was varied and it was found that at higher power the sample gets heated up and is elongating when it is strained. Hence, the power was fixed at 22 mW/cm^2 in all the experiments. Under different prestrains, virgin polymer shows random actuation behavior with both expansion and contraction. The photomechanical stress of the virgin SIS is very low when compared to graphene nanocomposites. The photomechanical stress of the nanocomposites increases with the graphene concentrations indicating that graphene has improved the IR actuation of the SIS. By comparing the photomechanical stress of virgin polymer with that of composites, we can easily understand the role of graphene as energy transfer unit. Graphene can absorb IR light and effectively transfer into the polymer matrix. The high IR absorption of graphene prepared by thermal reduction is attributed to the resonant induction by edge oxygen motion of mobile electrons localized in the vicinity of the oxygen.[38] Graphene can effectively transfer that absorbed energy into the polymer matrix, which makes a large difference in the photomechanical responses of the composite. The actuation is because of the triggering and subsequent release of stored mechanical energy in the material when in deformed state.

In the case of graphene/SIS nanocomposites, when prestrain is applied, contraction is exhibited on IR irradiation. Moreover, photoactuation of the composites is quite reversible [Figure 4(c)]. As the prestrain applied increases, the photomechanical stress of the nanocomposites increases. Similar results were reported in graphene/polydimethylsiloxane (PDMS) nanocomposites, which shows expansion at lower prestrain (10%) and contraction at higher prestrain.[29,30]. Though graphene improves the photomechanical properties of the SIS, there is an optimum graphene loading (1.5 wt%) beyond which the photomechanical stress decreases. This may be because of the decrease in the modulus of the nanocomposites by large, beyond the optimum filler loading. In order to confirm this, we have studied the mechanical properties of the nanocomposites (Table I). It is observed that graphene has dramatically increased the tensile strength and modulus of SIS. However, among the graphene/SIS nanocomposites, as the graphene concentration increases the mechanical properties decreases. At very low concentration of graphene (i.e., 0.1 wt%) the tensile strength of the SIS is increased to threefold that of virgin SIS. As the graphene concentration increases the tensile strength decreases and beyond 1.5 wt% of graphene loading the modulus

Table I. Mechanical Properties of Graphene/SIS Nanocomposites

Graphene loading (wt %)	Tensile strength (MPa)	Elongation at break (%)	Tensile modulus (MPa)
0	4.40	1898	0.23
0.1	13.06	2507	0.50
0.5	10.83	2879	0.38
1.0	9.50	2451	0.38
1.5	5.08	1907	0.24
2.0	5.80	2103	0.23

becomes comparable to that of virgin SIS. Because of the exfoliation of the graphitic layers, graphene has high surface area; hence, very low volume of graphene is sufficient for effective reinforcement. At higher volume percentage of graphene, the dilution effect predominates leading to decrease in mechanical properties. This reflects in the photomechanical characteristics of graphene/SIS nanocomposites, which shows decrease in the photomechanical stress beyond 1.5 wt % of graphene loading. The advantage of graphene is that very low filler concentration itself can convert SIS to a good photomechanical actuator. In addition, by controlling the prestrain given to the graphene/SIS nanocomposite photoactuators, one can control the photomechanical stress and strain to the required tune.

The photomechanical strain of the graphene/SIS nanocomposites is given in Figure 4(b). At lower prestrains, all the composites show almost similar strain on IR irradiation. A maximum strain of 3.1% (contraction) was obtained for 1.5 wt % of graphene/SIS nanocomposites. The effect of prestrain on photomechanical strain of the 1.5 wt % graphene/SIS nanocomposites is summarized in Table II. It is reported that, single layer graphene/PDMS nanocomposites showed a maximum strain of 1.6% contraction.[29] 2 wt % Graphene nanoplatelet-loaded PDMS showed maximum strain of less than 2.3%[30]. It can be found that higher photomechanical strain is obtained for graphene/SIS nanocomposites even at lower graphene concentration. Higher prestrain can be applied to SIS polymer when compared to PDMS matrix. Hence, a higher photomechanical stress and strain can be obtained if SIS is used for photoactuation.

Table II. Photomechanical Strain Behavior of 1.5 wt % Graphene–SIS Nanocomposites

	Photomechanical strain		
Prestrain (%)	Change in length (mm)	Strain (%)	Type of length change
0	−0.02	0.2	Expansion
10	0.00	0.0	-
22.4	0.03	0.3	Contraction
25.1	0.05	0.5	Contraction
30.5	0.06	0.6	Contraction
72.5	0.10	1.0	Contraction
98.4	0.18	1.8	Contraction
109.6	0.21	2.1	Contraction
159.2	0.31	3.1	Contraction

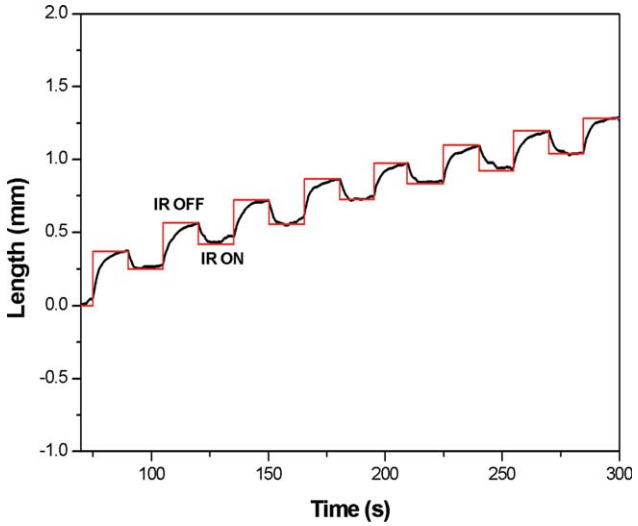

Figure 5. Multiple on/off IR cycles of 1.5 wt % graphene/SIS nanocomposite at a prestrain of 200 mN. [Color figure can be viewed in the online issue, which is available at wileyonlinelibrary.com.]

1.5 wt % graphene/SIS nanocomposite was subjected to multiple on/off IR cycles at a prestrain of 200 mN and the result is given in Figure 5. The prestrained nanocomposite sample contracts when IR light is switched on and relaxes when the light is switched off. The sample shows a reversible change in length. However, because of the creep deformation occurring in the SIS matrix, there is a marching in the length of the sample after each on–off cycle. It is also observed that the effect of creep deformation becomes less prominent after a few on/off cycles of light.

CONCLUSION

Graphene/SIS nanocomposite photoactuators were prepared by simple solvent-casting process. Photomechanical characteristics of graphene/SIS nanocomposites were studied at various prestrain. The actuation response of these nanocomposites was found to depend on prestrain and both photomechanical stress and strain increases with prestrain applied. A very low concentration of graphene gives good photomechanical characteristics to SIS and 1.5 wt % graphene/SIS nanocomposite was found to be having high photoactuation properties. Moreover, significant improvement in the mechanical properties of the SIS was observed with as low as 0.1 wt % loading of graphene. The graphene/SIS nanocomposites can be tuned to required actuation by controlling the graphene loading and prestrain applied. These graphene/polymer nanocomposites have great potential in biomedical application where remote control actuation and stimulus other than electrical signal is preferred.

ACKNOWLEDGMENTS

The authors gratefully acknowledge the financial support from Department of Science and Technology, Government of India.

REFERENCES

1. Ahir, S. V.; Terentjev, E. M. *Nature Mater.* **2005**, *4*, 491.
2. Liang, J.; Xu, Y.; Yi Huang; Zhang, L.; Wang, Y.; Ma, Y.; Li, F.; Guo, T.; Chen, Y. *J. Phys. Chem. C* **2009**, *113*, 9921.
3. Jiang, H.; Kelch, S.; Lendlein, A. *Adv. Mater.* **2006**, *18*, 1471.
4. Lu, S.; Ahir, S. V.; Terentjev, E. M.; Panchapakesan, B. *Appl. Phys. Lett.* **2007**, *91*, 103.
5. Yang, L.; Setyowati, K.; Li, A.; Gong, S.; Chen, J. *Adv. Mater.* **2008**, *20*, 2271.
6. Lu, S.; Panchapakesan, B. *Nanotechnology* **2005**, *16*, 2548.
7. Ahir, S. V.; Huang, Y.; Terentjev, E. M. *Polymer* **2008**, *49*, 3841.
8. Koerner, H.; Price, G.; Pearce, N. A.; Alexander, M.; Vaia R. A. *Nat. Mater.* **2004**, *3*, 115.
9. Levitsky, I. A.; Kanelos, P. T.; Woodbury, D. S.; Euler, W. B. *J. Phys. Chem. B* **2006**, *110*, 9421.
10. Lu, S.; Panchapakesan, B. *Nanotechnology* **2007**, *18*, 305502.
11. Ahir, S. V.; Squires, A. M.; Tajbakhsh, A. R.; Terentjev, E. M. *Phys. Rev. B* **2006**, *73*, 085420.
12. Ahir, S. V.; Terentjev, E. M. *Phys. Rev. Lett.* **2006**, *96*, 133902.
13. Geim, A. K. *Science* **2009**, *324*, 1530.
14. Geim, A. K.; Novoselov, K. S. *Nat. Mater.* **2007**, *6*, 183.
15. Zhang, N.; Li, R.; Zhang, L.; Chen, H.; Wang, W.; Liu, Y.; Wu, T.; Wang, X.; Wang, W.; Li, Y.; Zhao, Y.; Gao, J. *Soft Matter* **2011**, *7*, 7231.
16. Xie, X.; Bai, H.; Shi, G.; Qu, L. *J. Mater. Chem.* **2011**, *21*, 2057.
17. Park, S.; An, J.; Suk, J. W.; Ruoff, R. S. *Small* **2010**, *6*, 210.
18. Xie, X.; Qu, L.; Zhou, C.; Li, Y.; Zhu, J.; Bai, H.; Shi, G.; Dai, L. *ACS Nano* **2010**, *4*, 6050.
19. Zhu, S. E.; Shabani, R.; Rho, J.; Kim, Y.; Hong, B. H.; Ahn, J. H.; Cho, H. J. *Nano Lett.* **2011**, *11*, 977.
20. Shin, K. Y.; Hong, J. Y.; Jang, J. *Chem. Commun.* **2011**, *47*, 8527.
21. Lian, Y.; Liu, Y.; Jiang, T.; Shu, J.; Lian, H.; Cao, M. *J. Phys. Chem. C* **2010**, *114L*, 9659.
22. Jung, J. H.; Jeon, J. H.; Sridhar, V.; Il-Kwon, Oh. *Carbon* **2011**, *49*, 1279.
23. Kuila, T.; Bhadra, S.; Yao, D.; Kim, N. H.; Bose, S.; Lee, J. H. *Prog. Polym. Sci.* **2010**, *35*, 1350.
24. Stankovich, S.; Dikin, D. A.; Dommett, G. H. B.; Kohlhaas, K. M.; Zimney, E. J.; Stach, E. A.; Piner, R. D.; Nguyen, S. T.; Ruoff, R. S. *Nature* **2006**, *442*, 282.
25. Noorden, R. V. *Nature* **2006**, *442*, 228.
26. Ansari, S.; Kelarakis, A.; Estevez, L.; Giannelis, E. P. *Small* **2010**, *6*, 205.
27. Chen, D.; Tang, L.; Li, J. *Chem. Soc. Rev.* **2010**, *39*, 3157.
28. Ansari, S.; Giannelis, E. P. *J. Polym. Sci. Part B Polym. Phys.* **2009**, *47*, 888.
29. Loomis, J.; King, B.; Panchapakesan, B. *Appl. Phys. Lett.* **2012**, *100*, 073108.
30. Loomis, J.; King, B.; Burkhead, T.; Xu, P.; Bessler, N.; Terentjev, E. M.; Panchapakesan, B. *Nanotechnology* **2012**, *23*, 045501.
31. Liang, J.; Xu, Y.; Huang, Y.; Zhang, L.; Wang, Y.; Ma, Y.; Li, F.; Guo, T.; Chen, Y. *J. Phys. Chem.* **2009**, *113*, 9921.
32. Wu, C.; Feng, J.; Peng, L.; Ni, Y.; Liang, H.; Heb, L.; Xie, Y. *J. Mater. Chem.* **2011**, *21*, 18584.
33. Marcano, D. C.; Kosynkin, D. V.; Berlin, J. M.; Sinitskii, A.; Sun, Z.; Slesarev, A.; Alemany, L. B.; Lu, W.; Tour, J. M. *ACS Nano* **2010**, *4*, 4806.
34. Si, Y.; Samulski, E. T. *Nanoletters* **2008**, *8*, 1679.
35. Xu, Y.; Bai, H.; Lu, G.; Li, C.; Shi, G. *J. Am. Chem. Soc.* **2008**, *130*, 5856.
36. Li, D.; Muller, M. B.; Gilje, S.; Kaner, R. B.; Wallace, G. G. *Nat. Nanotechnol.* **2008**, *3*, 101.
37. Choi, E. Y.; Han, T. H.; Hong, J.; Kim, J. E.; Lee, S. H.; Kim, H. W.; Kim, S. O. *J. Mater. Chem.* **2010**, *20*, 1907.
38. Acik, M.; Lee, G.; Mattevi, C.; Chhowalla, M.; Cho, K.; Chabal, Y. J. *Nat. Mater.* **2010**, *9*, 840.